Effect of Thermal Radiation Pressure on Interplanetary Spacecraft

Yoshihide Sugimoto[1)] and Jozef C. van der Ha[2)]

[1)]*Department of Space and Astronautical Science, The Graduate University for Advanced Studies, Sagamihara, Japan*
[2)]*Consultant, Mission Design & Operations, Deming, WA, USA*

Abstract: Interplanetary spacecraft require precise predictions of their trajectory for achieving their mission targeting requirements. For the purpose of precise navigation, the detailed modeling of all small forces affecting the spacecraft's orbital motion is necessary. The dominating small forces on an interplanetary trajectory are planetary gravity perturbations and Solar Radiation Pressure. In addition to these traditional perturbations, the Thermal Radiation Pressure induced by the spacecraft surfaces can be an appreciable small force. This study focuses on the precise thermal analysis of the external surfaces by using a numerical Finite Element Method on three actual ESA interplanetary spacecraft, i.e. Rosetta, Mars Express, and Venus Express. This paper also presents the evaluations of the accelerations due to the Thermal Radiation Pressure.

摘要: 惑星間航行衛星のミッション達成において要求される制度を満たすために，非常に正確な航行軌道の推定が要求される．正確なナビゲーションのためには，宇宙機の軌道運動に影響を与える全ての微小力の影響モデルの構築が必要となる．惑星間航行軌道上にて支配的な微小力は太陽輻射圧であり，よく研究されている．近年では，宇宙機表面からの熱輻射が，同様に影響を与えうると考えられている．しかし，熱輻射に対する運動モデルは用いられない場合が多く，影響の大きさは未知である．当研究では正確な熱輻射モデルの構築を行い，実際に運用中の探査機を用いて熱輻射による加速度の評価を行う．

1. Introduction

Interplanetary spacecraft require precise predictions of their trajectory for achieving their mission targeting requirements, e.g., a gravity assist flyby or a rendezvous. For the purpose of precise navigation, the detailed modeling of all small forces affecting the spacecraft's orbital motion is required. The dominating small forces on an interplanetary trajectory are planetary gravity perturbations and Solar Radiation Pressure (SRP). In addition to these traditional perturbations, the Thermal Radiation Pressure (TRP) induced by the spacecraft surfaces can be an appreciable small force.

It has been reported that the existing SRP models have appreciable discrepancies in the predicted accelerations of up to 15% [1)]. These discrepancies cause serious problems for precise interplanetary navigation because only a few percent of acceleration error may result in a few thousand-km targeting error. Another aspect that must be kept in mind is the enormous ranges in solar distances that the interplanetary missions need to cope with. The wide variation in solar distances results in large differences of the incident solar radiation as well as in surface temperatures. This aggravates the precise predictions of the small perturbation forces.

In addition, the small effect from the TRP is usually not incorporated in the existing perturbation models. Nevertheless, an interplanetary spacecraft which travels close to the Sun or has a large surface area receives a significant heat flux from the Sun. The thermal radiation flux exerted by a high surface temperature on a large surface area has an appreciable perturbation effect on an interplanetary spacecraft [2)].

Therefore, the objective of this study is the establishment of the precise TRP effect on the interplanetary spacecraft. This result may solve the observed acceleration discrepancies and be helpful to improve the existing orbit propagators.

This study focuses on the precise thermal analysis of external surfaces using a numerical Finite Element Method (FEM) on three orbiting interplanetary spacecraft. This paper also presents the acceleration evaluations of the TRP.

2. Spacecraft

In this study, we provide the TRP results for three particular interplanetary spacecraft, i.e. Rosetta, Mars Express, and Venus Express [4)]. These spacecraft are designed and operated by European Space Agency (ESA) and are at present in their interplanetary trajectories to achieve their mission objectives.

The Rosetta spacecraft was launched by an Ariane-5 rocket in March 2004. Rosetta demonstrates several mission objectives during its approximately 10-year mission duration. Ultimately it will rendezvous and send a lander on the comet 67P/Churyumov-Gerasimenko[5)]. The Rosetta spacecraft is a large aluminum box with dimensions of 2.8×2.1×2.0 [m]. It has a number of scientific instruments [4)], a High-Gain Antenna (HGA) dish of 2.2 m diameter, and the lander *Philae* on the orbiter. Rosetta has also two enormous solar arrays of 32 m^2 area each. The total length of the two arrays plus the spacecraft body structure is enormous. It is about 32 m tip to tip.

Mars Express (MEX) was launched in June 2003 as the first European orbiter around Mars. MEX was launched by a Soyuz / Fregat. The Soyuz rocket has usually three stages but one stage, i.e. the fourth stage, can be added for particularly

demanding missions. In the case of MEX, the Fregat was used for the fourth stage. The spacecraft consists of an orbiter and a lander *Beagle2*. The orbiter consists of an aluminum honeycomb box-shaped structure and its dimensions are roughly 1.7 ×1.7 ×1.4 [m] with many scientific payloads (e.g., High Resolution Stereo Camera, Visible and Infrared Mineralogical Mapping Spectrometer, and Planetary Fourier Spectrometer) to survey and map the Mars surface and also its subsurface. The area of two solar arrays is about 5.8 m^2 each, which is much smaller than for Rosetta. This is because MEX travels to Mars and the distance from the Sun is much smaller compared to Rosetta's 5 AU maximum range.

Venus Express (VEX) was launched in November 2005 by a Soyuz/ Fregat like MEX. VEX has been built on the basis of the design experience of MEX. This made it quicker and cheaper to develop the spacecraft. Like MEX, also VEX is the first European spacecraft to visit Venus. VEX uses the same orbiter platform as MEX and the solar arrays are also basically the same. However, VEX requires only two pairs of solar panels on each solar array instead of the four on each array for MEX. This is because Venus has a closer orbit around the Sun than Mars. Thus, the VEX solar arrays receive a higher magnitude of solar radiation. Furthermore, the solar cells are separated by strips of Optical Solar Reflectors (OSRs) that help to reject the incoming heat flux from the solar radiation.

MEX and VEX fulfilled their nominal mission objective and they are in the extended mission phase in their respective planetary orbits. On the other hand, Rosetta is now entering into its hibernation phase before achieving its final objective, i.e. the rendezvous with the comet in 2014.

Table 1 summarizes the main properties of the three spacecraft studied here.

Table 1. Spacecraft Main Properties

Rosetta		
Size	Main Structure [m]	2.8×2.1×2.0
	Solar Arrays [m]	2.3×14
Mass	Total [kg]	3000
	Propellant [kg]	1670
Mars Express		
Size	Main Structure [m]	1.7×1.7×1.4
	Solar Arrays [m]	1.8×3.2
Mass	Total [kg]	1120
	Propellant [kg]	457
Venus Express		
Size	Main Structure [m]	1.7×1.6×1.4
	Solar Arrays [m]	1.8×1.6
Mass	Total [kg]	1245
	Propellant [kg]	570

3. Considered Perturbation Forces

In this chapter, we introduce the small forces induced by the SRP and TRP, which are considered in this research. These small forces act on an interplanetary trajectory. We do not provide the third-body perturbations, i.e., planetary gravitation, in this paper because these effects are well known and are well incorporated in existing orbit propagators.

3.1. SRP

The SRP is the most important perturbation force during interplanetary missions. Unlike the gravitational force, the SRP is a non-conservative force and it is mildly dependent upon the solar activity. For the purpose of predicting the SRP correctly, it is essential to understand how it interacts with the spacecraft[6].

The SRP originates from the energy intensity of the incoming radiation from the Sun. The solar intensity varies its magnitude in inverse proportion to the square of the solar distance, R_{Sun} in units of AU. The intensity energy at 1AU distance from the Sun is called the solar constant, S, and its magnitude is approximately 1367 W/m^2. Therefore, the intensity energy flux, q_{Sun}, when taking account of the solar distance is expressed as:

$$q_{Sun} = S/R_{Sun}^2 \ [\mathrm{W/m^2}] \tag{1.}$$

The photon momentum of the solar radiation per unit area is defined by Einstein's law relating energy, E, to mass, m, and the speed of light, c:

$$E = mc^2 \ [\mathrm{W/m^2}] \tag{2.}$$

The radiation pressure per unit area is the same as the photon momentum per unit area and the energy is equal to the intensity energy, q_{Sun}. In the result, the solar radiation exerts the pressure, p_{SRP}:

$$p_{SRP} = q_{Sun}/c \ [\mathrm{N/m^2}] \tag{3.}$$

Finally, the exerted pressure effects on the spacecraft surfaces exposed to the Sun act as a force, F_{SRP}, that can be expressed in terms of exposed surface area, A, surface reflectivity parameter, ρ, and the surface normal vector, $\mathbf{n}$, as follows:

$$\boldsymbol{F_{SRP}} = -p_{SRP} A \rho \mathbf{n} \ [\mathrm{N}] \tag{4.}$$

The negative sign in Eq. (4) indicates that the force is exerted in opposite direction to the Sun.

From Newton's second law of motion ("force equals mass times acceleration") the force induced by the SRP delivers the acceleration which we denote here the SRP acceleration, $\boldsymbol{a_{SRP}}$:

$$\boldsymbol{a_{SRP}} = (\boldsymbol{F_{SRP}}/m_s) \ [\mathrm{m/s^2}] \tag{5.}$$

where m_s denotes the spacecraft mass

The forces induced by the SRP through the different reflection process are separated in terms of particular surface reflectivity and the Sun incidence angle, θ, as follows:

$$\boldsymbol{F_{spe}} = -2p_{SRP} A \rho_{spe} \cos^2\theta \, \mathbf{n} \ [\mathrm{N}] \tag{6.}$$

$$\boldsymbol{F_{dif}} = -p_{SRP} A \rho_{dif} \cos\theta \, [2/3 \, \mathbf{n} + \boldsymbol{s}] \ [\mathrm{N}] \tag{7.}$$

$$\boldsymbol{F_{abs}} = -p_{SRP} A \alpha \cos\theta \, \boldsymbol{s} \ [\mathrm{N}] \tag{8.}$$

Ultimately, these individual reflection forces can be summarized in the total SRP force by the summation of equations Eq. (6)-(8):

$$\boldsymbol{F_{SRP}} = -p_{SRP} A \cos\theta \begin{bmatrix} (2\rho_{spe}\cos\theta + 2\rho_{dif}/3)\mathbf{n} \\ +(1+\rho_{spe})\boldsymbol{s} \end{bmatrix} \ [\mathrm{N}] \tag{9.}$$

Therefore, by means of Eq. (5) we can establish the Eq. (9) as follows:

$$\boldsymbol{a_{SRP}} = -\frac{p_{SRP} A \cos\theta}{m_s} \begin{bmatrix} (2\rho_{spe}\cos\theta + 2\rho_{dif}/3)\mathbf{n} \\ +(1+\rho_{spe})\boldsymbol{s} \end{bmatrix} \ [\mathrm{N}] \tag{10.}$$

3.2. TRP

A flat surface with temperature T emits thermal radiation diffusely. The thermal radiation produces the recoil force on the surface.

Fig. 1 illustrates the emission into a hypothetical hemisphere above a differential element area, dA [7]. The direction of emission will be specified in terms of the zenith angle, ξ, and the azimuth angle, φ. The area dA_n, through which the radiation passes, subtends a differential solid angle, $d\omega$, when viewed from a point on dA.

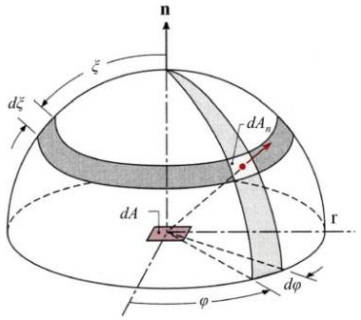

Fig. 1 Emission into a Hemisphere of Radius r

The emitted radiation flux, q_{rad}, from the surface is defined by the Stefan-Boltzmann law in terms of the surface emissivity, ε, the Stefan-Boltzmann constant, σ, and the surface temperature as follows:

$$q_{rad} = \varepsilon\sigma T^4 \ [\mathrm{W/m^2}] \tag{11.}$$

Following Lambert's cosine law, the emissive power, E_{rad}, emitted from an area can be expressed in terms of the zenith angle, the solid angle, and the emitted radiation flux as follows:

$$E_{rad} = (q_{rad}/\pi)\cos\gamma \, dAd\omega \ [\mathrm{W/m^2}] \tag{12.}$$

$$d\omega = dA_n/r^2 = \sin\gamma \, d\gamma d\varphi \tag{13.}$$

Eq. (12) gives the specific emissive power from a differential element area and the specific emissive power generates the recoil force for each solid angle. Similar to the SRP, the recoil force induced by the TRP can be calculated by means of the speed of light, c, through an integration process:

$$\boldsymbol{F_{TRP}} = \iiint (q_{rad}/\pi c)\cos^2\gamma \sin\gamma d\gamma d\varphi = -(2/3)(\varepsilon\sigma T^4/\mathrm{c})A\mathbf{n} \ [\mathrm{N}] \tag{14.}$$

Like the case of SRP, the acceleration, a_{TRP}, induced by the TRP is obtained from the force and the spacecraft mass as follows:

$$\boldsymbol{a_{TRP}} = -(2/3)(\varepsilon\sigma T^4/c)(A/m_s)\mathbf{n} \ [\mathrm{m/s^2}] \tag{15.}$$

Unlike the SRP acceleration, the TRP acceleration is also active on the shadowed surfaces, which are not exposed to the Sun. Therefore, it is essential to predict all surface temperatures. This is because all spacecraft surfaces including the shadowed surfaces have a non-zero temperature produces the small recoil force on the surfaces.

4. Thermal Analyses

The precise prediction of the TRP effect on the spacecraft requires the knowledge of the temperature distribution on the external spacecraft surfaces. Therefore, this chapter applies the thermal analyses to the actual spacecraft surfaces by both analytical and numerical methods.

Finally, we verify the effectiveness of the simulations on the actual spacecraft by comparing the simulation results and in flight temperatures.

4.1. Analytical Method

The analytical method is based on the straightforward balance of the heat input and output. These results provide a first-order estimate and give fundamental insights on the temperature prediction.

We assume that the heat input on the spacecraft is mainly by radiation from the outside. The spacecraft interior also generates heat for example, due to the On Board Computer (OBC) and other instruments. However, the Multi-Layer Insulator (MLI) isolating the spacecraft is well designed to control the internal temperature. Therefore, in general, the external surface may be regarded as independent of the interior temperature conditions.

There can be a number of sources of radiation acting on a spacecraft, for example solar radiation, Earth (or a planet) radiation, and albedo. The solar radiation is usually the major source of heat input on most spacecraft. In particular, during an interplanetary cruise trajectory, the incoming heat flux originates only from direct solar radiation.

The incoming heat flux, $q_{in,i}$, on the spacecraft surface is absorbed solar radiation. The incident solar radiation energy depends on the solar distance and also on the Sun incidence angle, θ, between the Sun vector, $\boldsymbol{s}$, and a surface normal vector, $\mathbf{n}$. Hence, the incoming heat flux is:

$$q_{in} = \alpha(S/R^2_{\boldsymbol{Sun}})\cos\theta \ [\mathrm{W/m^2}] \tag{16.}$$

where α is the surface absorptivity.

On the other hand, the outgoing heat flux is emitted thermal radiation from the surface. The temperature, Ti, of the arbitrary surface, i, radiates the infrared thermal radiation, $q_{out,i}$.

Therefore, the heat flux output, which follows Stephan-Boltzmann law, is expressed as follows:

$$q_{out,i} = \sum \varepsilon_i\sigma T_i^4 \ [\mathrm{W/m^2}] \tag{17.}$$

The shadowed surfaces require another calculation because there is no heat input from the Sun. Hence, the small amount of heat flux that crosses the MLI sheets from the body interior cannot be negligible for these surfaces.

The heat flux, q_{MLI}, through the MLI from the interior to cold deep-space environment is expected of the order of 5 $\mathrm{W/m^2}$ [1]. Therefore, by using Eq. (11), the shadowed surface temperature is expressed as follows:

$$T = \sqrt[4]{5/(\varepsilon\sigma)} \ [\mathrm{W/m^2}] \tag{18.}$$

When solving this equation we obtain the shadowed temperature of approximately -170℃ for studied spacecraft.

4.2. Numerical Method

The analytical method provides a valuable approximate prediction of the surface temperatures and also gives us useful fundamental insights. However, when regarding the spacecraft geometry, the heat transfer is not straightforward. We find that fractions of the heat fluxes are transferred between the body and the solar arrays. This heat flux transfer is the so called soak-back effect between body and solar arrays. The radiative

heat transfer between solar panels and spacecraft body, is obscured and hard to solve analytically. In addition to the soak-back effect, the spacecraft surfaces have lower temperatures at its edges because a small amount of heat flux is conducted to other surfaces and more heat flux radiates at the edges than at the center of the surface. Therefore, for performing a more precise thermal analysis, we established the numerical Finite Element Method (FEM) for the spacecraft by means of ANSYS software [8].

Figs. 2 represent an example image of Rosetta and the FEM model of Rosetta.

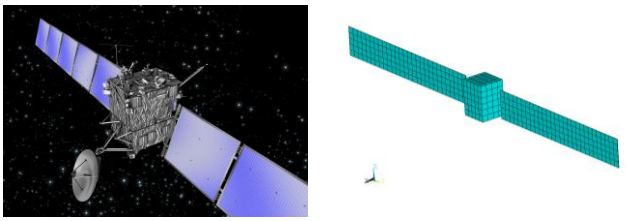

(a) Rosetta spacecraft (b) Rosetta Model

Fig. 2 Illustration of Rosetta and the FEM model

4.3. Thermal Results

Rosetta, MEX, and VEX are all three-axis stabilized spacecraft and have similar attitude control methods.

Fig. 3 illustrates the body model, the surface normal vectors, and the Sun vector. During most of the interplanetary cruise periods, the attitude of the spacecraft body is usually well controlled to keep the Sun vector within the X-Z plane. Thus, the Sun direction will essentially continuously be kept within the spacecraft body +X, +Z quadrant. Hence, the ±Y body surfaces receive no or only very little radiation input from the Sun. Therefore, the elevation angle, β, is the same as the Sun incidence angle for the +X body surface.

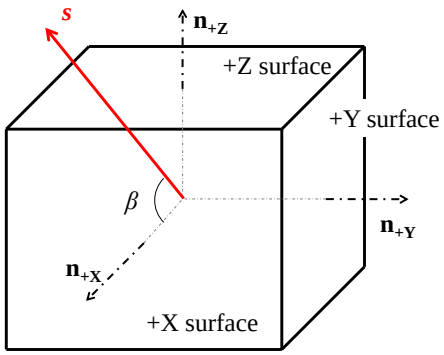

Fig. 3 Sun Vector Relative to Body Frame and Surface Normal Vectors

In addition to the body attitude, the spacecraft keeps its solar arrays, which are deployed along the body ±Y directions, pointing to the Sun by means of the solar array drive mechanism which rotates the solar arrays about the +Y and –Y axes. Thus, the Sun incidence angle relative to the front surface normal of the arrays can be taken as 0° . Therefore, it is obvious that only the array front surface receives solar radiation.

As an example, we show the results of the thermal analyses on the VEX spacecraft over its cruise phase. The spacecraft is designed to achieve a Venus orbit and it suffers a harsh heat environment.

Figs. 4 (a) and (b) demonstrate the external surface temperature results for the body and the arrays. Fig. 4 (a) shows the analytical and FEM results for the body surface and Fig. 4 (b) for the arrays. For both (a) and (b), the line curves show the analytical results and the dots show the FEM results.

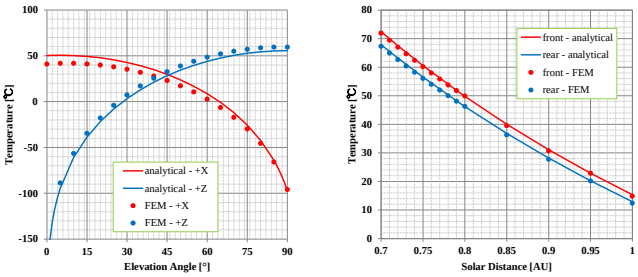

(a) Body Results (b) Solar Array Results

Fig. 4 VEX External Surface Temperatures of Body and Solar Array

Table 2 gives the summary of the analytical and FEM results at 1 AU distance from the Sun and two different elevation angles (i.e. 0 and 90°).

Table 2. Results of Predicted VEX Surface Temperatures at 1 AU

Elevation [°]	Surface		Temperature [℃]	
			Analytical	FEM
0	Body	+X	50.3	40.9
		+Z	-	-180.1
	Solar Array	Front	15.3	14.9
		Rear	12.9	12.4
90	Body	+X	-97.2	-96.0
		+Z	54.6	59.5
	Solar Array	Front	-	-
		Rear	-	-

The results show that the analytical and numerical methods predict similar temperatures for the surface. Thus, we conclude that the modeled FEM simulations are sufficient to predict the surface temperatures. However, we found temperature differences on the body surfaces. This may originate from the heat transfer between the neighboring surfaces which are not included in the analytical simulations.

We should mention that the arrays have always their front surfaces normal to the Sun. Therefore, we show them only in the 0 degree elevation angle.

In addition to the surface properties, we have the flight data of Rosetta's and VEX's arrays temperature histories. ESOC also distributes flight dynamics data on the TASC website [10] which includes the trajectory and attitude logs. Those results are useful for comparisons with predicted temperatures.

Fig. 5 provides the predicted VEX array temperatures and the VEX solar distance during the cruise phase start from 2005-11-09 to 2006-04-11. The red and blue curves show the arrays front and rear surface temperatures, respectively. The black cross symbol shows the VEX solar distance. The strong dependence of the temperatures on the solar distance can clearly be seen from this result.

Fig. 6 illustrates the predicted and measured arrays surface temperatures. The circular symbols show the measured temperatures from the two thermistors (T1, T2) on each of the arrays. The color curves notations for the predicted

temperatures are the same as in Fig. 5.

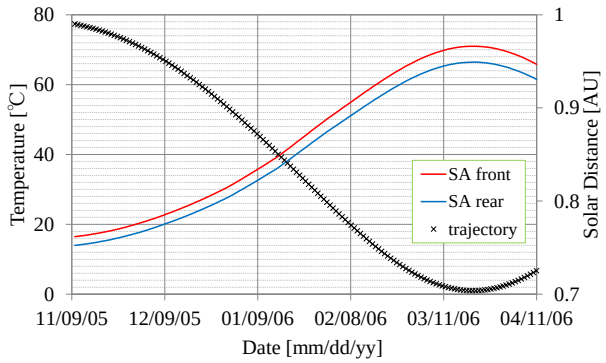

Fig. 5 Predicted VEX Solar Array Temperatures and Solar Distance

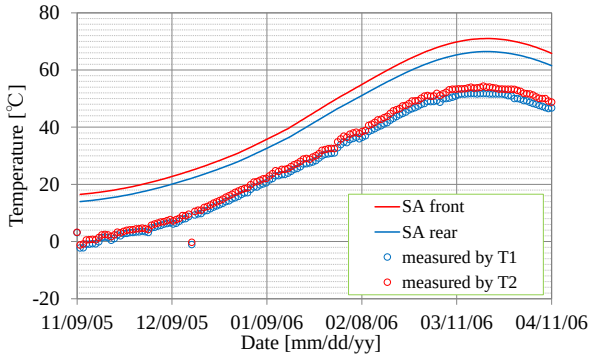

Fig. 6 Predicted vs Measured Array Surface Temperatures

4.3. Temperature Verification

The thermistors of the VEX arrays are attached on the rear side. Hence, the measured temperatures should coincide with the predicted rear surface temperatures. However, there are systematic temperature offsets between the predicted and measured temperatures. This is because the FEM simulations include only heat input from the Sun and do not include any other effects that may influence the surface temperatures. However, in reality, the arrays generate power and the solar cell conversion efficiency may vary depending on the cell temperature. Therefore, this source should be included for the exact prediction of the temperatures.

In order to include the power generation, we have to exclude the generated power, q_{pow}, from the initial heat input, q_{in}. After we get the modified heat input, q_{in}', we can perform the FEM simulation again with the modified heat input.

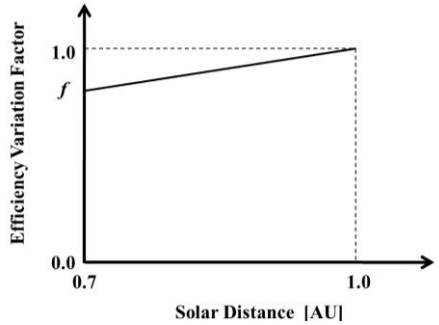

Fig. 7 Illustration of Solar Cell Efficiency Variation

The solar cell has a lower efficiency when its temperature is high and a higher efficiency when its temperature is low. Therefore, in this study, we assume that the variation of the solar cell efficiency behaves linearly as a function of the solar distance as shown in Fig. 7.

Fig. 8 shows the comparison results of the measured and modified predictions including the power conversion and cell efficiency variation. The optimum variation factor, *f*, is 0.95 in the results. The red and blue real lines are the modified temperature and the dotted lines are the initial temperature predictions. The real lines and circular symbols show very good matches to each other, and therefore, it can be concluded that the predictions and measurements match very well.

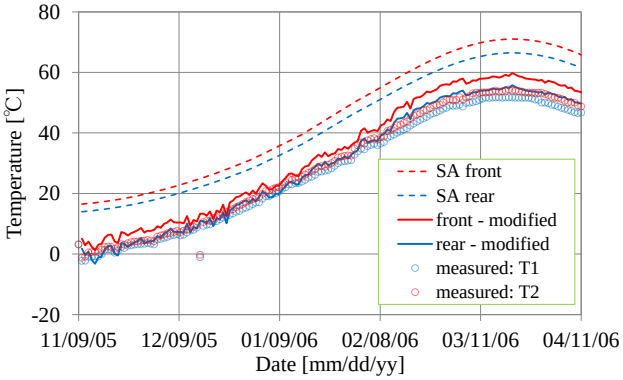

Fig. 8 Predicted vs Measured Temperatures under Realistic Conditions

5. Accelerations

In this chapter, we demonstrate the initial evaluation of the TRP acceleration by using the knowledge of the spacecraft properties and predicted temperatures. Thus, we construct a straightforward model for the acceleration of the spacecraft to compare the TRP acceleration with the SRP acceleration.

We show the results of the SRP and TRP acceleration for VEX calculated during the cruise phase. At first, we present the TRP acceleration results. Next, we compare the TRP results with the SRP results under the in same conditions in terms of the spacecraft elevation angle.

Fig. 9 shows the results of the predicted TRP accelerations. The pink and green curves show the 0 and 90 degrees of the elevation angles, respectively. The acceleration shows a maximum value when the attitude is 90-degree elevation angle and shows a minimum value when the elevation angle is 0-degree. This is because of the higher temperature and larger area of the +Z surface compared to the +X surface. This result also shows that the TRP accelerations are always within the two lines for in any attitude orientation.

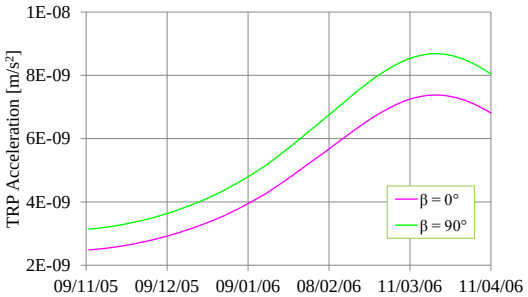

Fig. 9 Predicted TRP Acceleration during Cruise Phase

Fig. 10 includes the SRP acceleration in Fig. 9 in log scale. The color notations are the same as in Fig. 9 and the dotted lines show the SRP accelerations. The TRP accelerations are continuously much smaller than the SRP accelerations.

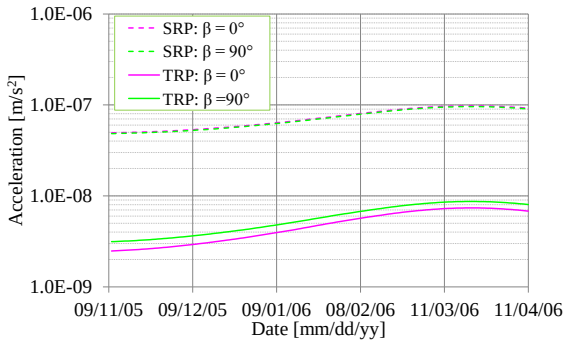

Fig. 10 Predicted TRP and SRP Accelerations

Table 3 summarizes the accelerations and the acceleration ratio of TRP/ SRP for the spacecraft, Rosetta, MEX, and VEX. Rosetta has completed five cruise phases by now so we show the average results.

Table 3. Summary of Spacecraft Acceleration Results

Accelerations [m/s^2]				Ratio [%]	
SRP ($\times 10^{-8}$)		TRP ($\times 10^{-9}$)			
Min.	Max	Min.	Max	Min.	Max
Rosetta (average: 2004-06-07 to 2009-09-13)					
5.04	10.7	2.98	7.90	5.36	7.13
Mars Express (2003-06-06 to 2003-12-19)					
3.29	6.90	1.94	5.25	5.91	7.61
Venus Express (2005-09-11 to 2006-11-04)					
4.84	9.77	2.48	8.68	5.05	9.05

For all spacecraft, we find that the acceleration ratio between the TRP and the SRP is about 5 to 9% in all case. Therefore, the magnitude of the TRP acceleration is the same as the observed acceleration discrepancy observed by ESA.

6. Conclusion

The precise thermal analyses using a numerical Finite Element Method (FEM) show the external surface temperature distributions. The predicted temperatures show excellent matches with the temperature histories measured by the thermistors.

From the exact temperature predictions, we calculate the accelerations induced by the Thermal Radiation Pressure (TRP). The calculated TRP acceleration is compared with the Solar Radiation Pressure (SRP) acceleration and the ratio of the TRP and SRP accelerations (TRP over SRP) are distributed in the range from 5 to 9%. This range of magnitudes fits very well with the observed acceleration discrepancies which are typically from 5 to 15%.

Acknowledgments

We acknowledge the contributions of Trevor Morley of ESA/ESOC in providing the spacecraft information, operational data, and other valuable advice on this research.

References

1) Van der Ha, J., and Stramaccioni, D.: Thermal Radiation on Deep-Space Trajectories, *AAS/AIAA Space Flight Mechanics Conference, Sna Diego, CA, USA*, 2010, paper AAS-10-226
2) Shoemaker, M., van der Ha, J., and Morley, T.: Reconstruction of Rosetta's Thermal Radiation Effects Using Orbit Determination Results, *AIAA/AAS Astrodynamics Specialist Conference, Toronto, Canada*, 2010, paper AIAA-2010-8263
3) Rievers, B., Bremer, S., List, M., Laemmerzahl, C., and Rath, H.: New Method for Accurate Thermal Disturbance Calculation with Application to Pioneer and Flyby Anomaly, *International Astronautical Conference, S. Daejeon, Korea*, 2009, paper IAC-09-C1.9.8
4) ESA space science http://www.esa.int/esaSC/index.html
5) Kueppers, M., et al.: Science Operations Planning of the Rosetta Encounter with Comet 67P/ Churyumov-Gerasimenko, *SpaceOps 2010 Conference*, AIAA paper 2010-2167, 2010.
6) Vallado, D. A.: *Fundamentals of Astronautics and Applications, Third Edition*, chap. 8.6.4, Microcosm Press, Haethorne, CA and Springer, New York, 2007, pp. 574-578
7) Incropera, F., Dewitt, D., Bergman, T., Lavine, A.: *Fundamentals of Heat and Mass Transfer , Sixth Edition*, John Wiley and Sons, New York, USA, 2005, pp. 724-762
8) ANSYS, Mechanical APDL, Software Package, Ver. 12.0, ANSYS, Inc., Canonsburg, USA, 2009
9) Sugimoto, Y., van der Ha, J., Rievers, B.: Thermal Radiation Model for Rosetta Spacecraft, *AIAA/AAS Astrodynamics Specialist Conference, Toronto, Canada*, 2010, paper AIAA-2010-7659
10) ESOC Flight Dynamics http://tasc.esa.int/index.html/